 

https://doi.org/10.1070/QEL17359

# Reversible plasmonic switching in a graphene nanoresonator loaded with a core–shell quantum dot

M.Yu. Gubin, A.V. Shesterikov, A.V. Prokhorov, V.S. Volkov

*Abstract.* **A model of an all-plasmonic switch based on a graphene waveguide integrated with a stub nanoresonator loaded with a quantum dot is considered. Using the full-wave numerical simulation, it is shown that successive on/off switching of the control surface plasmon–polariton wave at the input of the waveguide leads to a change in the phase of the signal plasmon–polariton wave in the nanoresonator by π. This causes reversible switching of the device operation regime – from almost complete blocking to stable transmission of the signal plasmon–polariton wave through the waveguide. The effect is implemented at rates of ∼0.5 THz for infrared electromagnetic waves localised in a device with a switching region of 40 × 20 nm.**

***Keywords:*** *graphene waveguide, nanoresonator, quantum dot, all-plasmonic switching.*

## 1. Introduction

Achievements of modern graphene technologies [1–3] and quantum nanoplasmonics [4, 5] allow expecting the practical implementation of fundamentally new information processing devices based on transistors operating at terahertz frequencies and having a size of a few nanometres. Such devices can be based on improved methods for controlling surface plasmon–polaritons (SPPs) [6–8] in 2D media and hybrid systems with high electron mobility and ultrafast nonlinearities [9–12]. For their fabrication, graphene materials loaded with semiconductor nanostructures, including semiconductor quantum dots (QDs), can be used [13, 14]. The simplest systems are systems in which QDs are located at such a distance from the 2D material that the structure of the electronic levels of the system does not undergo hybridisation.

The efficient interaction of QDs and the surface wave (QD-SPP coupling) in these systems is achieved when the strong coupling condition is satisfied [15, 16]. This means that the constant of the QD-SPP coupling exceeds the characteristic time of electron scattering in graphene [17] and the time of change in the spontaneous relaxation rate in the system [16, 17], as a result of which it becomes possible to effectively control the amplitude–phase characteristics of the SPP by changing the polarisation of the QD. At the same time, even when the strong coupling condition is met and the 'narrow' resonances for the SPP are achieved [18], the question of the reversibility and the influence of the rewritable memory effect on the functionality of such devices remains open [19].

In this work, we present the results of a study of the interaction of a semiconductor core–shell QD and SPP modes localised on the surface of a two-layer graphene. Two steady states of QD polarisation have been determined upon its interaction with two SPPs (signal/pump) using a ladder scheme of transitions between energy levels in a QD, which is placed in a graphene stub nanoresonator. It is shown that turning on (off) the SPP pump leads to a change in the level populations, as well as nonlinear QD polarisations and, as a consequence, to the possibility of controlling the nonlinear phase shift for the signal SPP. In particular, when the change of the signal SPP phase by π is induced by the pumping SPP, it is possible to implement reversible transitions from constructive interference in a stub nanoresonator to destructive one. The characteristic rate of such switching is ∼0.5 THz for a 40 × 20 nm nanoresonator. The discussed effects can be used to implement ultrafast plasmonic transistors and to design sensors and detectors with an 'instantaneous' response based on them.

## 2. Mathematical model of SPP propagation through a graphene waveguide integrated with a stub nanoresonator

Let us consider a model of a graphene waveguide coupled to a stub nanoresonator containing a core–shell QD (Fig. 1). In the absence of the resonator, the propagation constant $\beta$ for SPP localised on two graphene sheets obeys the dispersion equation [3]

$$-k_{\rm h}[\pm\exp(-k_{\rm h}d)-1]=2{\rm i}k_0c\varepsilon_{\rm d}\varepsilon_0/\sigma_{\rm g}, \qquad (1)$$

where $k_{\rm h}=\sqrt{\beta^2-k_0^2}$; $c$ is the speed of light; $k_0=2\pi/\lambda_0$; $\varepsilon_0$ is the dielectric constant; $\varepsilon_{\rm d}$ is the permittivity of the dielectric material between graphene sheets with a distance $d$ between them. The total conductivity of graphene $\sigma_{\rm g}=\sigma_{\rm inter}+\sigma_{\rm intra}$ is given by the Kubo formula and consists of the intraband conductivity

$$\sigma_{\rm intra}={\rm i}\frac{8\sigma_0kT/h}{\omega+{\rm i}/\tau}\left\{\frac{\mu_{\rm c}}{kT}+2\ln\left[\exp\left(-\frac{\mu_{\rm c}}{kT}\right)+1\right]\right\}$$

**M.Yu. Gubin, A.V. Shesterikov, A.V. Prokhorov** Vladimir State University, ul. Gor'kogo 87, 600000 Vladimir, Russia; e-mail: av_pr_vl_33@mail.ru;
**V.S. Volkov** Centre for Photonics and Two-Dimensional Materials, Moscow Institute of Physics and Technology, Institutskiy per. 9, 141701 Dolgoprudny, Moscow region, Russia

Received 27 May 2020
*Kvantovaya Elektronika* **50** (10) 976–983 (2020)
Translated by V.L. Derbov

and the interband conductivity

$$\sigma_{\text{inter}} = \mathrm{i}\frac{\sigma_0}{\pi}\ln\left[\frac{2|\mu_c| - (\omega + \mathrm{i}/\tau)\hbar}{2|\mu_c| + (\omega + \mathrm{i}/\tau)\hbar}\right],$$

where $k$ is the Boltzmann constant; $T$ is the temperature; $\mu_c$ is the chemical potential; $1/\tau$ is the scattering rate; $\sigma_0 = \pi e^2/(2h)$; and $e$ is the electron charge.

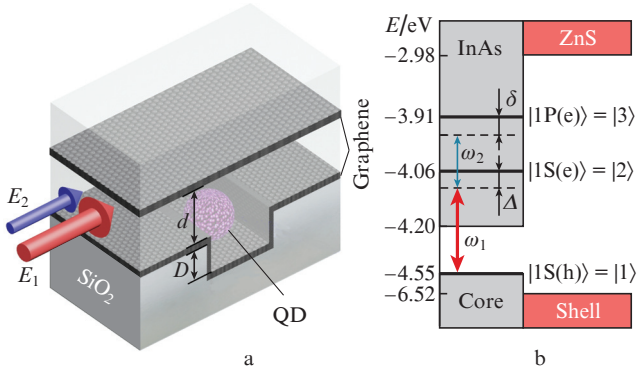


**Figure 1.** (Colour online) (a) Model of a stub nanoresonator based on two structured graphene sheets and a core–shell QD placed in a dielectric and (b) scheme of the ladder-type interaction of a SPP and a core--shell InAs/ZnS QD with a radius of $a_{QD} = 9.9$ nm; the working energy levels in the QD are located in the valence band ($E_{|1\rangle} = -4.55$ eV) and in the conduction band ($E_{|2\rangle} = -4.063$ eV and $E_{|3\rangle} = -3.908$ eV).

To simulate the operation of the device, we choose the effective graphene thickness $\Delta_g = 2$ nm (which corresponds to the discretisation step in the finite difference time domain (FDTD) method [20] and significantly differs from the true graphene sheet thickness equal to ~0.33 nm); other parameters are as follows: $\mu_c = 0.6$ eV, $\tau = 0.9$ ps, $\varepsilon_d = 2.022$, signal field wavelength $\lambda_2 = 8.04$ μm, and pump wavelength $\lambda_1 = 2.56$ μm. For the chosen parameters, the intraband conductivity exceeds the interband conductivity for the pump field and dominates over it for the signal field (Fig. 2). At the same time, to take into account the contribution of the interband conductivity in the FDTD simulation, its approximation by the Padé formula is required:

$$\bar{\sigma}_{\text{inter}} = \frac{a_0 + a_1(\mathrm{i}\omega) + a_2(\mathrm{i}\omega)^2}{1 + b_1(\mathrm{i}\omega) + b_2(\mathrm{i}\omega)^2}, \qquad (2)$$

the coefficients in which are determined by fitting with the reference frequencies $\omega_{p1}$, $\omega_{p2}$, and $\omega_{p3}$ [21]. As a result of this approximation, the coefficients $a_0 = 2.346 \times 10^{-8}$, $a_1 = -2.112 \times 10^{-20}$, $a_2 = 9.589 \times 10^{-39}$, $b_1 = -6.745 \times 10^{-19}$, and $b_2 = 1.007 \times 10^{-31}$ were obtained near $\lambda_2$ using three reference wavelengths: $\lambda_{p1} = 7.2$ μm, $\lambda_{p2} = 8.2$ μm and $\lambda_{p3} = 9.2$ μm (Fig. 2a).

To estimate the type of coupling between SPP and two-layer graphene the following parameter is used:

$$\xi = \mathrm{Re}\left(\frac{\sigma_g}{\mathrm{i}c\varepsilon_0\varepsilon_d k_0}\right).$$

The case $d > \xi$ corresponds to the weak coupling of SPP with graphene, in which the dispersion curves for two-layer graphene have a hyperbolic shape and almost coincide with the dispersion curves for single-layer graphene. On the contrary,

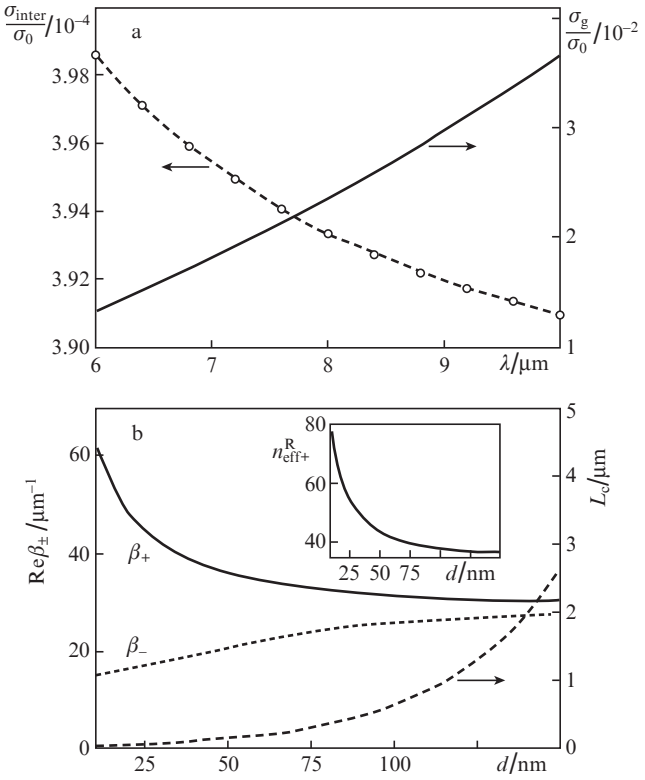


**Figure 2.** (a) Frequency dependences of the total ($\sigma_g$) and interband ($\sigma_{\text{inter}}$) conductance with the results of the Padé approximation (circles); (b) dependences of the propagation constants $\beta_\pm$ and the interaction length $L_c = 2\pi/(2\sqrt{2}\,|\beta_- - \beta_+|)$ for the signal SPP versus the distance $d$ between graphene sheets. The inset shows the dependence of the effective refractive index on the distance $d$.

the case $d < \xi$ corresponds to a strong SPP-graphene coupling, for which the dispersion curves differ significantly from their monolayer graphene analogues [22]. To satisfy the strong coupling condition between SPP and graphene for the signal field with $\lambda_2$, we choose $d = 20$ nm and, taking into account the fact that for the used graphene $\xi = 71$ nm, we obtain a very good localisation of the plasmon–polariton mode at the characteristic wavelength $\lambda_{SPP+} = 135.5$ nm. Note that Eqn (1) has two solutions, $\beta_+$ and $\beta_-$ (Fig. 2b), corresponding to symmetric and antisymmetric modes [22], but we will consider only $\beta_+$, since in this case the electromagnetic field is strongly localised in the gap between graphene sheets. This will be required in the future to satisfy the strong coupling condition between the SPP and the QD placed in the gap between the sheets. Then, determining the effective refractive index of the graphene waveguide in the form $n_{\text{eff}\pm} = n^{\text{R}}_{\text{eff}\pm} + \mathrm{i}n^{\text{I}}_{\text{eff}\pm} = \beta_\pm/k_0$, it is possible to estimate for SPP both the wavelength $\lambda_{SPP+} = 2\pi/\mathrm{Re}\beta_+$ and its characteristic propagation length $\bar{L}_{SPP+} = \lambda_0/(4\pi\,\mathrm{Im}\,n_{\text{eff}+})$ in a waveguide consisting of two parallel graphene sheets. In particular, the parameter $\bar{L}_{SPP+}$ will be 3.7 μm for the signal SPP.

The stub resonators considered below are commonly used to filter the electromagnetic signal at fixed wavelengths [23]. In this work, it is proposed to insert an active centre (QD or quantum well, dye molecule, and other chromophores) into such a resonator, which can be used for efficient control of the phase shift of the signal field interacting with this centre. This can be achieved by changing the polarisations of the corresponding transitions between energy levels of the centre under

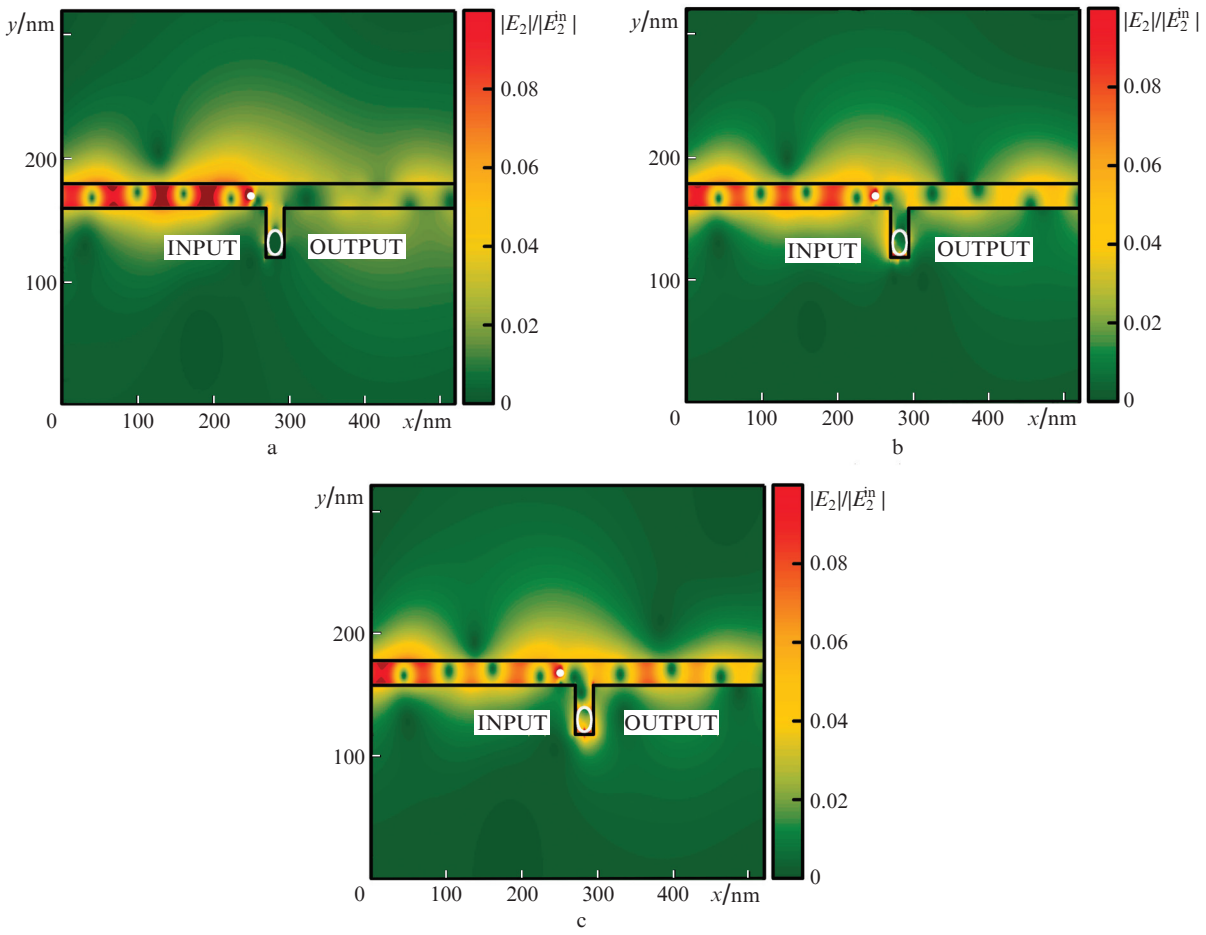


**Figure 3.** (Colour online) Contour plots of spatial distributions of the resulting electric field component $(E_{2x}^2 + E_{2y}^2)^{1/2}$ for the signal SPP at times $t$ = (a) 5 ps (with the pump on), (b) 12 ps (at the time of changing the transmission regime) and (c) 15 ps (with pump off). The white point between the graphene sheets is the location of the field source (magnetic dipole), the white circle inside the resonator is the location of the QD.

the action of an additional pump field, which can be described using the density matrix formalism and based on the analysis of the stability of nonlinear systems [24].

To begin with, we choose the height $D$ of the stub resonator so that the signal field is tuned to the interference maximum and is not blocked by the resonator. This is possible if the 'plasmon' path of the signal SPP in the resonator $\Delta S = (2D + d)n_{\text{eff}+}^{\text{R}}$ will be equal to an integer number of wavelengths, i.e., $l\lambda_0$, where $l = 0, 1, 2, \ldots$. Then, choosing $l = 1$, we obtain $D$ = 40 nm (the resonator width is 24 nm), and the signal field will freely propagate through the region of the waveguide containing the nanoresonator (Fig. 3c).

## 3. Reversible switching of the transmittance of the signal SPP mode through a graphene waveguide integrated with a QD-loaded nanoresonator

We assume that in the nanoresonator loaded with a core–shell InAs/ZnS QD, the C-scheme of plasmon–exciton interaction of the ladder type with two SPP modes is realised (see Fig. 1b). The control pump field $E_1$ (determined by the set of components, i.e., $E_1^2 = E_{1x}^2 + E_{1y}^2$) is tuned to the interband transition 1S(h) → 1S(e), and the signal field $E_2$ is tuned to the intraband transition 1S(e) → 1P(e). The resonance frequencies of the corresponding transitions can be obtained in the form (see Fig. 1)

$$\omega_{12} = \frac{eE_{\text{g}}}{\hbar} + \frac{2\hbar k_{1;0}}{D_{\text{QD}}^2}\left(\frac{1}{m_{\text{e}}} + \frac{1}{m_{\text{h}}}\right), \tag{3a}$$

$$\omega_{23} = \frac{2\hbar}{D_{\text{QD}}^2 m_{\text{e}}}(k_{1;1}^2 + k_{1;0}^2), \tag{3b}$$

where $E_{\text{g}}$ = 0.35 eV is the band gap width; $m_{\text{e}} = 0.026m_0$ and $m_{\text{h}} = 0.41m_0$ are the effective masses of an electron and a hole in InAs, respectively; $m_0$ is the mass of a free electron; and $k_{1;1}$ = 4.439 and $k_{1;0} = \pi$ are the roots of the Bessel function. According to expression (3b), to implement resonant interactions with the SPP signal mode at a wavelength $\lambda_2$ = 8.04 μm, the QD radius $a_{\text{QD}} = D_{\text{QD}}/2$ should be 9.9 nm. Then, the pump wavelength $\lambda_1$ = 2.56 μm will be precisely tuned to the interband resonance in accordance with expression (3a) and the condition $\omega_{12} = \omega_1$.

The performed numerical simulation demonstrates the rapid decay of the pump SPP under weak coupling conditions ($\xi$ = 6 nm) for the electromagnetic field at a wavelength $\lambda_1$ in a graphene waveguide. However, even in this case, the pump SPP intensity is sufficient to provide induced polarisation at the 1S(h) → 1S(e) transition in the QD.

The dipole moment of the intraband transition in the QD can be approximately estimated as $\mu_{32} = 0.433ea_{QD}\Lambda$, where $\Lambda = 3\varepsilon_{ZnS}/(2\varepsilon_{ZnS} + \varepsilon_{InAs})$, $\varepsilon_{InAs} = 12.3$ is the permittivity of the QD core, and $\varepsilon_{ZnS} = 8.3$ is the permittivity of the shell. At the same time, the dipole moment of the interband transition can be found from the expression

$$\mu_{21}^2 = \frac{e^2}{6m_0\omega_1^2}\left(\frac{m_0}{m_e} - 1\right)\frac{E_g e(E_g + \Delta_s)}{E_g + 2\Delta_s/3},$$

where $\Delta_s = 0.43$ eV is the energy of the spin–orbit splitting for InAs. The calculated values of the parameters for the considered InAs/ZnS QD are as follows: $\mu_{32} = 5.91 \times 10^{-28}$ C m and $\mu_{21} = 14.9 \times 10^{-29}$ C m.

In the absence of field $E_1$, the 1S(e) energy level is not populated; therefore, steady-state solutions for the matrix elements of transitions in the QD are equal to zero values, i.e., $\bar{\rho}_{21} = \bar{\rho}_{32} = 0$. In this situation, the signal field freely propagates through the region containing the nanoresonator (Fig. 3c). The instantaneous switching on of the field $E_1$ leads to an increase in the oscillating polarisation at the 1S(e) → 1P(e) transition. In the process of subsequent evolution, the system stabilises with new steady-state solutions for polarisation (see Appendix):

$$\bar{\rho}_{32} = -\frac{i\Omega_2\left(\Omega_1^2 n_{21} + D_1 D_2 n_{32} + \Omega_2^2 n_{32}\right)}{\Omega_1^2 D_1 + D_1 D_2 \Gamma_{32} + \Omega_2^2 \Gamma_{32}},$$

$$\bar{\rho}_{21} = -\frac{i\Omega_1\left(\Omega_1^2 n_{21} + \Omega_2^2 n_{32} + D_2 n_{21}\Gamma_{32}\right)}{\Omega_1^2 D_1 + D_1 D_2 \Gamma_{32} + \Omega_2^2 \Gamma_{32}}, \quad (4)$$

where $\Omega_1 = g_1 B$ and $\Omega_2 = g_2 a$ are the Rabi frequencies of the pump and the signal SPP modes; $B$ and $a$ are the amplitudes of the corresponding SPPs; $D_1 = i\Delta + \gamma_{21}$; $D_2 = i\delta + \gamma_{31} + \gamma_{32}$; $\Gamma_{32} = i(\delta - \Delta) + \gamma_{21} + \gamma_{32} + \gamma_{31}$; $\bar{n}_{21} = \bar{\rho}_{22} - \bar{\rho}_{11}$; $\bar{n}_{32} = \bar{\rho}_{33} - \bar{\rho}_{22}$; and $\bar{\rho}_{11}$, $\bar{\rho}_{22}$, and $\bar{\rho}_{33}$ are steady-state solutions for the level populations. It should be noted that at a subwavelength distance between QDs and graphene, the relaxation parameters change significantly [16, 25–27]. The magnitude of this change can be determined either exactly for a simplified case, when the chromophore is located near a flat conducting layer [26], or within the framework of an approximate calculation of the local density of optical states (LDOS) [28] based on the existing field distribution in the nanoresonator. Here we used the first approach and obtained an estimate of the relaxation parameters: $\gamma_{32(31)} = 1.43 \times 10^{12}$ s$^{-1}$ and $\gamma_{21} = 5 \times 10^{11}$ s$^{-1}$ [18]. In fact, the accurate calculation of the spontaneous relaxation rate for a non-point emitter in a complex-shaped resonator is a fundamental problem that requires refinement and has nontrivial solutions even for simple geometries [27].

To study the dynamics of a coupled SPP-QD system, we use a combined approach [29] based on the numerical solution of a system of differential equations for the density matrix (A4) and numerical simulation of the electromagnetic field by the FDTD method [20]. Within the framework of this approach, we assume that the plasmon–exciton coupling parameter

$$g_{1(2)}(\boldsymbol{r}) = \sqrt{\frac{\omega_{1(2)}}{\hbar\varepsilon_0 V_{eff\,1(2)}}}\varkappa_{1(2)}(\boldsymbol{r})\mu_{21(32)},$$

where the coefficient $\varkappa_{1(2)}(\boldsymbol{r}) = E_{1(2)}(\boldsymbol{r})/E_{1(2)}^{max}$ specifies the field distribution at the point with coordinate $\boldsymbol{r}$ where the QD is located, and $V_{eff\,1(2)} = \lambda_{SPP+1(2)}^3$ corresponds to the effective mode volume. Determining the values of these parameters directly from the simulation results for the field in the resonator, we obtain $g_1 = 6.575 \times 10^{11}$ s$^{-1}$ and $g_2 = 1.472 \times 10^{12}$ s$^{-1}$.

The switching principle (Fig. 3) is based on controlling the phase shift of the signal SPP mode in the resonator by changing the polarisation values (4) via the pump field variation. This phase shift can be calculated using the formula $\Delta\phi = (2\pi/\lambda_2)\mathrm{Re}[n_{QD}]D_{QD}$, where the effective refractive index of the QD has the form $n_{QD} \approx \chi_{QD}/2$ and is expressed through its susceptibility $\chi_{QD} = [N\mu_{32}/(\varepsilon_0 E_2)]\bar{\rho}_{32}$ ($N$ is the concentration of charge carriers). Hence, the QD permittivity induced by the external field can be represented as $\varepsilon_{QD} = 1 + \chi_{QD}$. For the case $a = 1$ and $B = 10$, we obtain that the phase shift $\Delta\phi = \pi$ required for the transition from constructive interference to destructive one can be realised at frequency detunings $\Delta_m = -6.156 \times 10^{12}$ s$^{-1}$ and $\delta_m = 1.697 \times 10^{13}$ s$^{-1}$ (in this case, $\mathrm{Re}\bar{\rho}_{32} = 0.0318$ and $\mathrm{Im}\bar{\rho}_{32} = 0.0065$).

To test the device operation, we use the gating of the nanoresonator by the pump field at a rate of $2\pi/\tau_d$ with the signal field turned on. In this case, the pump field amplitude changes abruptly from zero to $E_1^{max}$ and back at the moments of time $t = m\tau_d$ ($\tau_d = 10$ ps, $m = 0, 1, \ldots$), leading to oscillations of the permittivity $\varepsilon_{QD}^R$ of the quantum dot (Fig. 4b).

Numerical simulation of the electromagnetic field was carried out taking into account the phase shift that changes following the polarisation of the signal SPP mode in the resonator. As a numerical criterion for the transmission of the signal SPP through the waveguide, we chose the transmittance, which is defined as the ratio of the integrated $E_2$ field intensities from different sides of the nanoresonator, i.e., $K_{tr} = (S_{tr}/S_{total}) \times 100\%$, where $S_{total}$ is the integrated field intensity inside the waveguide, including the resonator region, and $S_{tr}$ is the integrated field intensity to the right of the resonator centre, but within the waveguide. Thus, at $E_1 = 0$, the transmittance $K_{tr}$ is 33.3%, decreasing to 7.6% at $E_1 = E_1^{max}$ (Fig. 4). An important feature of the presented scheme is the achievement of 'narrow' plasmon resonances in the stub nanoresonator, which provide a high transmittance of the signal field when the pump field is off. Switching on the pump field leads to prolonged oscillations of the QD permittivity. At the same time, the transmittance decreases to a minimum

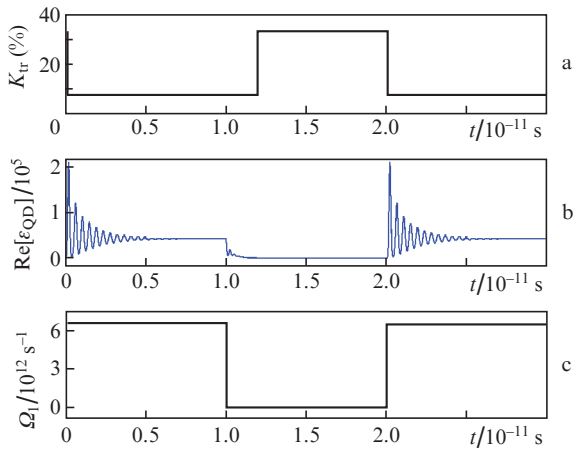


**Figure 4.** Time dependences of (a) the transmittance $K_{tr}$ of the signal field through a graphene waveguide integrated with a stub resonator, (b) QD permittivity and (c) Rabi frequency $\Omega_1$.

value almost 'instantly', which is associated with violation of the resonance conditions even with small changes in $\varepsilon_{QD}^{R}$ (Fig. 4). The reverse transition of the system when the pump field is turned off occurs in a time $\tau_{sw} = 2$ ps, which provides a switching rate of 0.5 THz.

## 4. Possibilities of technical implementation of all-plasmonic switches with QDs

The design and fabrication of all-plasmonic switches require separate consideration. The fabrication of such devices is possible using the existing modern technologies, but utilising a combination of several different experimental techniques at once. In particular, dielectric substrates made of silica glass $SiO_2$ or aluminium oxide $Al_2O_3$, on the surface of which grooves of the required size and shape are made, can be a basis for the production of devices [30]. The deposition of a graphene layer on the surface of such a structured dielectric can be realised using plasma-enhanced chemical vapour deposition (PECVD [31]). In this case, the deposition of graphene occurs when two precursors are combined, which are hydrogen and methane at a pressure of 10 mTorr and a temperature of 500–900 °C. However, the problem of the stability of the graphene layer thickness when it covers such bulk elements as a stub nanoresonator requires an experimental study similar to [32] for dielectric strips. The issues of graphene modification [33], including the fabrication of doped graphene with altered chemical potential and electron scattering rate, are also a particular problem.

The next stage is associated with loading QDs into a nanoresonator, which can be performed by using the technique of micro- and nanomanipulation using the tip of an atomic force microscope [34]. The simplified technology consists in depositing a QD layer on the graphene surface with their subsequent mechanical removal from the surface in such a way as to leave single QDs situated in the nanoresonator.

Coating the graphene layer with a dielectric is the most difficult stage, since it requires the use of low-temperature methods to preserve the integrity of the graphene layer. In particular, using the technique of atomic layer deposition (ALD [35]) with such precursors as $AlCl_3$ and $H_2O$, $Al_2O_3$ can be deposited at a temperature of 200–400 °C. The use of trimethylamine and water allows one to reduce the graphene deposition temperature to 125 °C [36] and to 100 °C [37]. It should be noted that the quality of adhesion of materials significantly depends on the state of the graphene surface, taking into account its initially hydrophobic nature. To solve this problem, methods of functionalisation of the graphene surface are used, in particular, the deposition of a thin (1–2 nm thick) Al layer on the graphene surface [38], which is completely oxidised during atomic layer deposition. This determines the qualitative grapheme–insulator interface without deteriorating the electron mobility in graphene. The subsequent stages, i.e. the deposition of a second graphene layer to produce the waveguide structure and its covering with a dielectric, require an alternate use of the PECVD and ALD methods. In the absence of access to ALD, the technological chain can be rebuilt to use the method of electron beam evaporation for the deposition of a dielectric on graphene [39]. However, its use requires a rigidly specified geometry of the location of the source and the sample (the sample is at the top of the chamber), which may be unacceptable for the considered nanoresonator + QD device.

Let us focus on the details of the development and application of an effective near-field SPP source for the considered system. Under experimental conditions, the available near-field sources are mainly represented by near-field microscopy devices (near-field scanning microscope, NSM) equipped with tips of various configurations. Usually this is a pointed tip of an optical waveguide, which can have various geometries, sizes and topologies. The simplest case is a rounded tip, in which, depending on the radius of its curvature, various configuration resonances can be excited corresponding to different moments of the electromagnetic field [40]. In accordance with this, the tips can be dipole sources (electric and magnetic [41]), quadrupole sources, etc. However, even when using NSM needles based on highly refractive materials [42], their size remains incommensurate with the characteristic scale ($40 \times 20$ nm) of a plasmonic switch (see Fig. 1a).

A partial solution of the problem can be provided by using all-dielectric nanoantennas [43], as well as hybrid nanostructures, including quantum nanowires [44], which make it possible to capture and convert the energy of the electromagnetic field at the nanoscale. Such systems are used to fabricate nanolasers [45], but can also be used as near-field sources with specified classical [46] and quantum [47, 48] characteristics and can be integrated into plasmonic schemes (see Fig. 1a).

Another important problem is the localisation of SPPs propagating over the graphene surface in a narrow region along the $z$ axis. This problem can be solved purely technically using micro- and nanostructured substrates based on a combination of Si and $SiO_2$ layers. In those areas where SPP is required to be localised, Si with a thin buffer layer of $SiO_2$ serves as a substrate for graphene, and monolithic $SiO_2$ plays this role in the remaining areas. Thus, Si and the graphene layer above it act as an extended capacitor: when a voltage is applied to it, the chemical potential of graphene decreases in comparison with that for regions above monolithic $SiO_2$ [49–51]. As a result, a waveguide effect arises: SPPs are localised and propagate only along the graphene regions located above Si, which can be used to create complex internode connections in the system [30] and data buses for plasmonic circuits.

## 5. Conclusions

In this work, we propose a model and discuss the fabrication of an all-plasmonic reversible switch based on a graphene stub resonator loaded with a core–shell QD. It should be noted that the relatively small propagation lengths of SPPs in graphene systems compared with those in metal–insulator–semiconductor structures [52] significantly limit the scaling of such devices to full-fledged integrated circuits [53]. At the same time, the presented model can be of fundamental importance for the development of both individual high-speed switches and ultrafast sensors based on them. In the latter case, a plasmonic switch can be used to quickly trigger a certain operating algorithm in the electronic part of the circuit when an optical signal is applied to one of its inputs. In addition, advances on the way to achieving high-temperature conductivity of graphene [54, 55] give hope for a solution to the problem of SPP rapid damping in graphene. In this case, additional technical difficulties lie in the maintaining of superconductivity upon contact of a two-dimensional material with a substrate [56]. The solution of such problems requires the use of a new paradigm in the creation of functional optical and optoelectronic devices based on two-

dimensional materials with unique physical characteristics [57–59].

***Acknowledgements.*** The authors are grateful to A.B. Evlyukhin for useful discussions. This work was supported by the Ministry of Science and Higher Education of the Russian Federation (0714-2020-0002). A.V. Shesterikov greatfully acknowledges the support from the Foundation for Assistance to Small Innovative Enterprises(Agreement 14287GU/2019, UMNIK).

## Appendix. Mathematical model of the ladder scheme of SPP-QD coupling

The Hamiltonian of SPP-QD interaction can be represented as

$$H = H_0 + H_v, \tag{A1a}$$

where

$$H_0 = \hbar[\omega_{12}|2\rangle\langle 2| + (\omega_{12}+\omega_{23})|3\rangle\langle 3|] \tag{A1b}$$

is the unperturbed Hamiltonian and

$$H_v = -\hbar(\tilde{\Omega}_1|2\rangle\langle 1| + \tilde{\Omega}_1^*|1\rangle\langle 2| + \tilde{\Omega}_2|3\rangle\langle 2| + \tilde{\Omega}_2^*|2\rangle\langle 3|) \tag{A1c}$$

is the Hamiltonian of the interaction between the semiconductor QD and two SPP modes in accordance with the ladder interaction scheme (see Fig. 1b); $|1\rangle \equiv |1S(h)\rangle$ is the ground energy state of a hole in the valence band; $|2\rangle \equiv |1S(e)\rangle$ and $|3\rangle \equiv |1P(e)\rangle$ are the electronic states in the conduction band; $\tilde{\Omega}_1$ and $\tilde{\Omega}_2$ are the Rabi frequencies of the pump and signal SPP modes; and $\omega_{12}$ and $\omega_{23}$ are the frequencies of interband and intraband transitions, respectively.

The evolution of the presented system is described using the Liouville equation

$$\frac{\partial\tilde{\rho}}{\partial t} = -\frac{i}{\hbar}[H,\tilde{\rho}] - \hat{\Gamma}, \tag{A2a}$$

where

$$\tilde{\rho} = \tilde{\rho}_{11}|1\rangle\langle 1| + \tilde{\rho}_{22}|2\rangle\langle 2| + \tilde{\rho}_{33}|3\rangle\langle 3| + \tilde{\rho}_{12}|1\rangle\langle 2| + \tilde{\rho}_{21}|2\rangle\langle 1| + \tilde{\rho}_{23}|2\rangle\langle 3| + \tilde{\rho}_{32}|3\rangle\langle 2| + \tilde{\rho}_{13}|1\rangle\langle 3| + \tilde{\rho}_{31}|3\rangle\langle 1| \tag{A2b}$$

is the density matrix of the QD states;

$$\hat{\Gamma} = \gamma_{21}(|2\rangle\langle 2|\tilde{\rho} - 2|1\rangle\langle 2|\tilde{\rho}|2\rangle\langle 1| + \tilde{\rho}|2\rangle\langle 2|) + \gamma_{32}(|3\rangle\langle 3|\tilde{\rho} - 2|2\rangle\langle 3|\tilde{\rho}|3\rangle\langle 2| + \tilde{\rho}|3\rangle\langle 3|) + \gamma_{31}(|3\rangle\langle 3|\tilde{\rho} - 2|1\rangle\langle 3|\tilde{\rho}|3\rangle\langle 1| + \tilde{\rho}|3\rangle\langle 3|) \tag{A2c}$$

is the Lindblad superoperator describing the process of spontaneous relaxation in the system; $\gamma_{ij}$ are the rates of spontaneous relaxation of the corresponding transitions; and $i, j = 1, 2, 3$ and $i \neq j$.

Using expressions (A1) and (A2), we obtain the following system of equations for the elements of the density matrix:

$$\begin{aligned}
\dot{\tilde{\rho}}_{11} &= i\tilde{\Omega}_1^*\tilde{\rho}_{21} - i\tilde{\Omega}_1\tilde{\rho}_{12} + 2\gamma_{21}\tilde{\rho}_{22} + 2\gamma_{31}\tilde{\rho}_{33},\\
\dot{\tilde{\rho}}_{22} &= i\tilde{\Omega}_1\tilde{\rho}_{12} - i\tilde{\Omega}_1^*\tilde{\rho}_{21} + i\tilde{\Omega}_2^*\tilde{\rho}_{32} - i\tilde{\Omega}_2\tilde{\rho}_{23} - 2\gamma_{21}\tilde{\rho}_{22} + 2\gamma_{32}\tilde{\rho}_{33},\\
\dot{\tilde{\rho}}_{33} &= i\tilde{\Omega}_2\tilde{\rho}_{23} - i\tilde{\Omega}_2^*\tilde{\rho}_{32} - 2\gamma_{32}\tilde{\rho}_{33} - 2\gamma_{31}\tilde{\rho}_{33},\\
\dot{\tilde{\rho}}_{12} &= i\tilde{\Omega}_1^*\tilde{\rho}_{22} + i\omega_{12}\tilde{\rho}_{12} - i\tilde{\Omega}_1^*\tilde{\rho}_{11} - i\tilde{\Omega}_2\tilde{\rho}_{13} - \gamma_{21}\tilde{\rho}_{12},\\
\dot{\tilde{\rho}}_{21} &= -i\tilde{\Omega}_1\tilde{\rho}_{22} - i\omega_{12}\tilde{\rho}_{21} + i\tilde{\Omega}_1\tilde{\rho}_{11} + i\tilde{\Omega}_2^*\tilde{\rho}_{31} - \gamma_{21}\tilde{\rho}_{21},\\
\dot{\tilde{\rho}}_{13} &= i\tilde{\Omega}_1^*\tilde{\rho}_{23} + i(\omega_{12}+\omega_{23})\tilde{\rho}_{13} - i\tilde{\Omega}_2^*\tilde{\rho}_{12} - \gamma_{31}\tilde{\rho}_{13} - \gamma_{32}\tilde{\rho}_{13},\\
\dot{\tilde{\rho}}_{31} &= -i\tilde{\Omega}_1\tilde{\rho}_{32} - i(\omega_{12}+\omega_{23})\tilde{\rho}_{31} + i\tilde{\Omega}_2\tilde{\rho}_{21} - \gamma_{31}\tilde{\rho}_{31} - \gamma_{32}\tilde{\rho}_{31},\\
\dot{\tilde{\rho}}_{23} &= i\omega_{23}\tilde{\rho}_{23} + i\tilde{\Omega}_1\tilde{\rho}_{13} + i\tilde{\Omega}_2^*\tilde{\rho}_{33} - i\tilde{\Omega}_2^*\tilde{\rho}_{22} - \tilde{\rho}_{23}(\gamma_{21}+\gamma_{32}+\gamma_{31}),\\
\dot{\tilde{\rho}}_{32} &= -i\omega_{23}\tilde{\rho}_{32} - i\tilde{\Omega}_1^*\tilde{\rho}_{31} - i\tilde{\Omega}_2\tilde{\rho}_{33} + i\tilde{\Omega}_2\tilde{\rho}_{22} - \tilde{\rho}_{32}(\gamma_{21}+\gamma_{32}+\gamma_{31}).
\end{aligned} \tag{A3}$$

Next, we apply the slowly varying amplitude approximation to introduce new variables

$$\tilde{\rho}_{12} = \rho_{12}\exp(i\omega_1 t),\ \ \tilde{\rho}_{23} = \rho_{23}\exp(i\omega_2 t),$$

$$\tilde{\rho}_{13} = \rho_{13}\exp[i(\omega_1+\omega_2)t],\ \tilde{\rho}_{11} \equiv \rho_{11},\ \tilde{\rho}_{22} \equiv \rho_{22},\ \ \tilde{\rho}_{33} \equiv \rho_{33},$$

$$\tilde{\Omega}_1 = \Omega_1\exp(i\omega_1 t),\ \ \tilde{\Omega}_2 = \Omega_2\exp(i\omega_2 t),$$

where $\omega_{1(2)}$ are the frequencies of the pump(signal) SPP mode.

Then the system of equations (A3) is transformed to a new form:

$$\begin{aligned}
\dot{\rho}_{11} &= i\Omega_1^*\rho_{21} - i\Omega_1\rho_{12} + 2\gamma_{21}\rho_{22} + 2\gamma_{31}\rho_{33},\\
\dot{\rho}_{22} &= i\Omega_1\rho_{12} - i\Omega_1^*\rho_{21} + i\Omega_2^*\rho_{32} - i\Omega_2\rho_{23} - 2\gamma_{21}\rho_{22} + 2\gamma_{32}\rho_{33},\\
\dot{\rho}_{33} &= i\Omega_2\rho_{23} - i\Omega_2^*\rho_{32} - 2\gamma_{32}\rho_{33} - 2\gamma_{31}\rho_{33},\\
\dot{\rho}_{12} &= i\Omega_1^*\rho_{22} + i\Delta\rho_{12} - i\Omega_1^*\rho_{11} - i\Omega_2\rho_{13} - \gamma_{21}\rho_{12},\\
\dot{\rho}_{21} &= -i\Omega_1\rho_{22} - i\Delta\rho_{21} + i\Omega_1\rho_{11} + i\Omega_2^*\rho_{31} - \gamma_{21}\rho_{21},\\
\dot{\rho}_{13} &= i\Omega_1^*\rho_{23} + i\delta\rho_{13} - i\Omega_2^*\rho_{12} - \gamma_{31}\rho_{13} - \gamma_{32}\rho_{13},\\
\dot{\rho}_{31} &= -i\Omega_1\rho_{32} - i\delta\rho_{31} + i\Omega_2\rho_{21} - \gamma_{31}\rho_{31} - \gamma_{32}\rho_{31},\\
\dot{\rho}_{23} &= i(\delta-\Delta)\rho_{23} + i\Omega_1\rho_{13} + i\Omega_2^*\rho_{33} - i\Omega_2^*\rho_{22} - \rho_{23}(\gamma_{21}+\gamma_{32}+\gamma_{31}),\\
\dot{\rho}_{32} &= -i(\delta-\Delta)\rho_{32} - i\Omega_1^*\rho_{31} - i\Omega_2\rho_{33} + i\Omega_2\rho_{22} - \rho_{32}(\gamma_{21}+\gamma_{32}+\gamma_{31}),
\end{aligned} \tag{A4}$$

where $\Delta = \omega_{12} - \omega_1$; and $\delta = \omega_{12} + \omega_{23} - \omega_1 - \omega_2$. Introducing new variables $n_{21} = \rho_{22} - \rho_{11}$ and $n_{32} = \rho_{33} - \rho_{22}$, system (A4) can be represented in the form:

$$\dot{n}_{21} = 2i\Omega_1\rho_{12} - 2i\Omega_1^*\rho_{21} + i\Omega_2^*\rho_{32} - i\Omega_2\rho_{23} -$$

$$-4\gamma_{21}\rho_{22}+2(\gamma_{32}-\gamma_{31})\rho_{33}, \tag{A5a}$$

$$\dot{n}_{32}=2\mathrm{i}\Omega_2\rho_{23}-2\mathrm{i}\Omega_2^*\rho_{32}-\mathrm{i}\Omega_1\rho_{12}+\mathrm{i}\Omega_1^*\rho_{21}$$
$$-4\gamma_{32}\rho_{33}-2\gamma_{31}\rho_{33}+2\gamma_{21}\rho_{22}, \tag{A5b}$$

$$\dot{\rho}_{21}=-\mathrm{i}\Omega_1 n_{21}-\mathrm{i}\Delta\rho_{21}+\mathrm{i}\Omega_2^*\rho_{31}-\gamma_{21}\rho_{21}, \tag{A5c}$$

$$\dot{\rho}_{32}=-\mathrm{i}\Omega_2 n_{32}-\mathrm{i}(\delta-\Delta)\rho_{32}-\mathrm{i}\Omega_1^*\rho_{31}$$
$$-(\gamma_{21}+\gamma_{32}+\gamma_{31})\rho_{32}, \tag{A5d}$$

$$\dot{\rho}_{31}=-\mathrm{i}\Omega_1\rho_{32}-\mathrm{i}\delta\rho_{31}+\mathrm{i}\Omega_2\rho_{21}-(\gamma_{31}+\gamma_{32})\rho_{31}. \tag{A5e}$$

Considering the steady-state regime of SPP-QD coupling (i.e., the case when the time derivatives are zero), we find $\rho_{31}$ from Eqn (A5e) in the form

$$\bar{\rho}_{31}=\frac{\mathrm{i}\Omega_2\bar{\rho}_{21}-\mathrm{i}\Omega_1\bar{\rho}_{32}}{\mathrm{i}\delta+\gamma_{31}+\gamma_{32}}, \tag{A6}$$

where $\bar{\rho}_{21}$, $\bar{\rho}_{32}$, and $\bar{\rho}_{31}$ are the steady-state values of the polarisation at the corresponding transitions. Substituting $\bar{\rho}_{31}$ into (A5c) and (A5d), we obtain the expressions

$$\begin{aligned}0&=-\mathrm{i}\Omega_1 n_{21}-\rho_{21}\left(\mathrm{i}\Delta+\gamma_{21}+\frac{|\Omega_2|^2}{\mathrm{i}\delta+\gamma_{31}+\gamma_{32}}\right)\\&+\frac{\Omega_1\Omega_2^*\rho_{32}}{\mathrm{i}\delta+\gamma_{31}+\gamma_{32}},\\0&=-\mathrm{i}\Omega_2 n_{32}+\frac{\Omega_1^*\Omega_2\rho_{21}}{\mathrm{i}\delta+\gamma_{31}+\gamma_{32}}\\&-\rho_{32}\left[\gamma_{21}+\gamma_{32}+\gamma_{31}+\mathrm{i}(\delta-\Delta)+\frac{|\Omega_1|^2}{\mathrm{i}\delta+\gamma_{31}+\gamma_{32}}\right].\end{aligned} \tag{A7}$$

Solving system (A7), we determine the steady-state solutions $\bar{\rho}_{21}$ and $\bar{\rho}_{32}$ in the form:

$$\begin{aligned}\bar{\rho}_{21}&=-\frac{\mathrm{i}\Omega_1(|\Omega_1|^2\bar{n}_{21}+|\Omega_2|^2\bar{n}_{32}+D_2\bar{n}_{21}\Gamma_{32})}{|\Omega_1|^2D_1+D_1D_2\Gamma_{32}+|\Omega_2|^2\Gamma_{32}},\\\bar{\rho}_{32}&=-\frac{\mathrm{i}\Omega_2(|\Omega_1|^2\bar{n}_{21}+D_1D_2\bar{n}_{32}+|\Omega_2|^2\bar{n}_{32})}{|\Omega_1|^2D_1+D_1D_2\Gamma_{32}+|\Omega_2|^2\Gamma_{32}}.\end{aligned} \tag{A8}$$

Substituting (A8) into Eqns (A4), one can find steady-state solutions for the level populations:

$$\begin{aligned}\bar{\rho}_{11}&=1-\bar{\rho}_{22}-\bar{\rho}_{33},\\\bar{\rho}_{22}&=\frac{|\Omega_1|^2}{A}\{|\Omega_2|^4\Gamma_1\gamma_{32}+|\Omega_2|^2\{\delta^2[\Gamma_2^2+(\Gamma_2+\Gamma_3)\gamma_{21}]\\&-2\delta\Delta\Gamma_2\gamma_{32}+\Gamma_2(\Gamma_1^2\Gamma_2+\Delta^2\gamma_{32}+\Gamma_1\gamma_{21}\gamma_{32})\\&+(\Gamma_1\Gamma_2+\gamma_{21}\gamma_{32})|\Omega_1|^2\}+B\},\\\bar{\rho}_{33}&=\frac{|\Omega_2|^2|\Omega_1|^2}{A}\{|\Omega_2|^2\Gamma_1^2+[(\delta-\Delta)^2+\Gamma_1^2]\Gamma_2\gamma_{21}\\&+\Gamma_1\gamma_{21}|\Omega_1|^2\},\end{aligned} \tag{A9}$$

where

$$\begin{aligned}A&=|\Omega_2|^6\Gamma_1\Gamma_3+B(\Delta^2+\gamma_{21}^2+2|\Omega_1|^2)\\&+|\Omega_2|^4\{[\delta^2+\Delta^2+\Gamma_1(\Gamma_1+2\Gamma_3)]\Gamma_2\gamma_{21}\\&-2\delta\Delta(\Gamma_1\Gamma_3+\Gamma_2\gamma_{21})+[\gamma_{21}^2+(\Gamma_1+\Gamma_2)(\Gamma_1-\gamma_{31})]|\Omega_1|^2\}\\&+|\Omega_2|^2\{\delta^2[(2\Gamma_2^2+\Gamma_1\Gamma_3)\gamma_{21}^2+\Delta^2(\Gamma_1\Gamma_3+4\Gamma_2\gamma_{21})\\&+2(\Gamma_1^2+\gamma_{21}\gamma_{31})|\Omega_1|^2]+2\delta\Delta\Gamma_2[-\gamma_{21}(\delta^2+\Delta^2+\Gamma_1^2\\&+2\Gamma_2\gamma_{21})+(\gamma_{31}-\gamma_{32})|\Omega_1|^2]+\Delta^2\Gamma_2(\Gamma_1\Gamma_2\Gamma_3+2\Gamma_2\gamma_{21}^2\\&+\gamma_{32}|\Omega_1|^2)+(\Gamma_1\Gamma_2+|\Omega_1|^2)[\Gamma_2(2\Gamma_1+\Gamma_3)\gamma_{21}^2\\&+(\Gamma_1^2+\Gamma_2^2+2\gamma_{21}\gamma_{32})|\Omega_1|^2]\};\\B&=\Gamma_2\gamma_{21}\{[(\delta-\Delta)^2+\Gamma_1^2](\delta^2+\Gamma_2^2)\\&+2[\delta(\Delta-\delta)+\Gamma_1\Gamma_2]|\Omega_1|^2+|\Omega_1|^4\};\text{ and}\end{aligned}$$

$$\Gamma_1=\gamma_{21}+\gamma_{31}+\gamma_{32};\ \ \Gamma_2=\gamma_{31}+\gamma_{32};\ \ \Gamma_3=\gamma_{21}+\gamma_{31}.$$

Thus, expressions (A8) and (A9) allow tuning the required regime of interaction between the QD and the signal SPP by controlling the parameters of this interaction via the intensity of the SPP pumping.

## References


1. Freitag M., Chizhova L.A., Nemes-Incze P., Woods C.R., Gorbachev R.V., Cao Y., Geim A.K., Novoselov K.S., Burgdörfer J., Libisch F., Morgenstern M. *Nano Lett*., **16** (9), 5798 (2016).
2. Tamagnone M., Slipchenko T.M., Moldovan C., Liu P.Q., Centeno A., Hasani H., Zurutuza A., Ionescu A.M., Martin-Moreno L., Faist J., Mosig J.R., Kuzmenko A.B., Poumirol J.-M. *Phys. Rev. B*, **97** (24), 241410(R) (2018).
3. Liang X., Giacometti V., Ismach A., Harteneck B.D., Olynick D.L., Cabrini S. *Appl. Phys. Lett*., **96** (1), 013109 (2010).
4. Bozhevolnyi S.I., Martin-Moreno L., Garcia-Vidal F. *Quantum Plasmonics* (Cham: Springer International Publishing, 2017).
5. Radko I.P., Volkov V.S., Beermann J., Evlyukhin A.B., Søndergaard T., Boltasseva A., Bozhevolnyi S.I. *Laser Photonics Rev*., **3** (6), 575 (2009).
6. Pshenichnyuk I.A., Kosolobov S.S., Maimistov A.I., Drachev V.P. *Quantum Electron*., **48** (12), 1153 (2018) [*Kvantovaya Elektron*., **48** (12), 1153 (2018)].
7. Pshenichnyuk I.A., Nazarikov G.I., Kosolobov S.S., Maimistov A.I., Drachev V.P. *Phys. Rev. B*, **100** (19), 195434 (2019).
8. Dzedolik I.V., Skachkov S. *J. Opt. Soc. Am. A*, **36** (5), 775 (2019).
9. Stebunov Y.V., Arsenin A.V., Volkov V.S., in *Chemically Derived Graphene: Functionalization, Properties and Applications* (Cambridge: The Royal Society of Chemistry Publishing, 2018) Ch. 12.
10. Jiang Y., Lin X., Low T., Zhang B., Chen H. *Laser Photon. Rev*., **12**, 1800049 (2018).
11. Motlagh S., Apalkov V., Stockman M.I. arXiv: 1812.08812v1 (2018).
12. Nesterov M.L., Bravo-Abad J., Nikitin A.Y., Garcia-Vidal F.J., Martin-Moreno L. *Laser Photon. Rev*., **7** (2), 1 (2012).
13. Kim B.-S., Neo D.C.J., Hou B., Park J., Cho Y., Zhang N., Hong J., Pak S., Lee S., Sohn J., Assender H.E., Watt A.A.R., Cha S., Kim J. *ACS Appl. Mater. Interfaces*, **8** (22), 13902 (2016).
14. Zhang Y., Cao M., Song X., Che Y., Ding X., Zhang G., Yao J., Dai H., Wang J. *J. Phys. Chem. C*, **119** (37), 21739 (2015).
15. Cui G., Raymer M.G. *Phys. Rev. A*, **73** (5), 053807 (2006).

16. Koppens F.H.L., Chang D.E., García de Abajo F.J. *Nano Lett*., **11** (8), 3370 (2011).
17. Fedorov A.V., Baranov A.V., Rukhlenko I.D., Perova T.S., Berwick K. *Phys. Rev. B*, **76** (4), 045332 (2007).
18. Gubin M.Yu., Leksin A.Yu., Shesterikov A.V., Volkov V.S., Prokhorov A.V. *Appl. Surf. Sci*., **506**, 144814 (2019).
19. Chen W.-C. *Electrical Memory Materials and Devices* (Cambridge: The Royal Society of Chemistry Publishing, 2016).
20. Sullivan D.M. *Electromagnetic Simulation Using the FDTD Method* (New York: Wiley–IEEE Press, 2000).
21. Mock A. *Opt. Mater. Express*, **2**, 771 (2012).
22. Aliofkhazraei M., Ali N., Milne W.I., Ozkan C.S., Mitura S., Gervaso J.L. *Graphene Science Handbook. Electrical and Optical Properties* (Boca Raton: CRC Press, 2016).
23. Lin X.S., Huang X.G. *Opt. Lett*., **33** (23), 2874 (2008).
24. Ryzhov I.V., Malikov R.F., Malyshev A.V., Malyshev V.A. *Phys. Rev. A*, **100** (3), 033820 (2019).
25. Larkin I.A., Stockman M.I., Achermann M., Klimov V.I. *Phys. Rev. B*, **69** (12), 121403(R) (2004).
26. Novotny L., Hecht B. *Principles of Nano-Optics* (New York: Cambridge University Press, 2006).
27. Gubin M.Yu., Gladush M.G., Prokhorov A.V. *Opt. Spectrosc*., **126** (1), 83 (2019) [*Opt. Spektrosk*., **126** (1), 78 (2019)].
28. De Wilde Y., Formanek F., Carminati R., Gralak B., Lemoine P.-A., Joulain K., Mulet J.-P., Chen Y., Greffet J.-J. *Nature*, **444**, 740 (2006).
29. Gubin M.Yu., Leksin A.Yu., Shesterikov A.V., Prokhorov A.V., Volkov V.S. *Nanomaterials*, **10**, 122 (2020).
30. Vakil A., Engheta N. *Science*, **332** (6035), 1291 (2011).
31. Kim Y.S., Joo K., Jerng S.-K., Lee J.H., Yoon E., Chun S.-H. *Nanoscale*, **6** (17), 10100 (2014).
32. Grigorenko A., Polini M., Novoselov K. *Nat. Photonics*, **6**, 749 (2012).
33. Pivovarov P.A., Frolov V.D., Zavedeev E.V., Konov V.I. *Quantum Electron*., **47** (11), 1017 (2017) [*Kvantovaya Elektron*., **47** (11), 1017 (2017)].
34. Ratchford D., Shafiei F., Kim S., Gray S.K., Li X. *Nano Lett*., **11** (3), 1049 (2011).
35. Alles H., Aarik J., Kozlova J., Niilisk A., Rammula R., Sammelselg V., in *Graphene – Synthesis, Characterization, Properties and Applications* (Rijeka: InTech, 2011) Ch. 7.
36. Jeon J.H., Jerng S.-K., Akbar K., Chun S.-H. *ACS Appl. Mater. Interfaces*, **8** (43), 29637 (2016).
37. Nayfeh O.M., Marr T., Dubey M. *IEEE Electron. Device Lett*., **32** (4), 473 (2011).
38. Kim S., Nah J., Jo I., Shahrjerdi D., Colombo L., Yao Z., Tutuc E., Banerjee S.K. *Appl. Phys. Lett*., **94**, 062107 (2009).
39. Hwang H.J., Cheng L., Lucero A.T., Lee B.H., Kim J. *Proc. 11th Int. Conf. IEEE NMDC* (Toulouse, France, 2016).
40. Evlyukhin A.B., Reinhardt C., Evlyukhin E., Chichkov B.N. *J. Opt. Soc. Am. B*, **30** (10), 2589 (2013).
41. Le Feber B., Rotenberg N., Kuipers L. *Nat. Commun*., **6**, 6695 (2014).
42. Terekhov P.D., Baryshnikova K.V., Shalin A.S., Karabchevsky A., Evlyukhin A.B. *Opt. Lett*., **42** (4), 835 (2017).
43. Sinev I.S., Komissarenko F.E., Mukhin I.S., Petrov M.I., Iorsh I.V., Belov P.A., Samusev A.K. *Nanosystems: Phys., Chem., Mathem*., **9** (5), 609 (2018).
44. Ho J., Tatebayashi J., Sergent S., Fong C.F., Iwamoto S., Arakawa Y. *ACS Photonics*, **2** (1), 165 (2014).
45. Noginov M.A., Zhu G., Belgrave A.M., Bakker R., Shalaev V.M., Narimanov E.E., Stout S., Herz E., Suteewong T., Wiesner U. *Nature*, **460** (7259), 1110 (2009).
46. Linkov P., Samokhvalov P., Vokhmintsev K., Zvaigzne M., Krivenkov V.A., Nabiev I. *JETP Lett*., **109** (2), 112 (2019) [*Pis'ma Zh. Eksp. Teor. Fiz*., **109** (2), 108 (2019)].
47. Gubin M.Yu., Shesterikov A.V., Karpov S.N., Prokhorov A.V. *Phys. Rev. B*, **97** (8), 085431 (2018).
48. Shesterikov A.V., Gubin M.Yu., Karpov S.N., Prokhorov A.V. *JETP Lett*., **107** (7), 435 (2018) [*Pis'ma Zh. Eksp. Teor. Fiz*., **107** (7), 459 (2018)].
49. Jian-Rong H., Jiu-Sheng L., Guo-Hua Q. *J. Infrared, Millimeter, Terahertz Waves*, **37** (7), 668 (2016).
50. Bahadori-Haghighi S., Ghayour R., Sheikhi M.H. *Plasmonics*, **14** (2), 447 (2018).
51. Jin Q., Li X., Chen J., Gao S. *Sci. Rep*., **7** (1), 12290 (2017).
52. Fedyanin D.Y., Yakubovsky D.I., Kirtaev R.V., Volkov V.S. *Nano Lett*., **16** (1), 362 (2015).
53. Ni G.X., McLeod A.S., Sun Z., Wang L., Xiong L., Post K.W., Sunku S.S., Jiang B.-Y., Hone J., Dean C.R., Fogler M.M., Basov D.N. *Nature*, **557** (7706), 530 (2018).
54. Zhou J., Sun Q., Wang Q., Jena P. *Phys. Rev. B*, **92** (6), 064505 (2015).
55. Ichinokura S., Sugawara K., Takayama A., Takahashi T., Hasegawa S. *ACS Nano*, **10** (2), 2761 (2016).
56. Kong X.-T., Bai B., Dai Q. *Opt. Lett*., **40** (1), 1 (2015).
57. Britnell L., Ribeiro R.M., Eckmann A., Jalil R., Belle B.D., Mishchenko A., Kim Y.-J., Gorbachev R.V., Georgiou T., Morozov S.V., Grigorenko A.N., Geim A.K., Casiraghi C., Castro Neto A.H., Novoselov K.S. *Science*, **340** (6138), 1311 (2013).
58. Palacios-Berraquero C., Barbone M., Kara D.M., Chen X., Goykhman I., Yoon D., Ott A.K., Beitner J., Watanabe K., Taniguchi T., Ferrari A.C., Atature M. *Nat. Commun*., **7**, 12978 (2016).
59. Yakubovsky D.I., Stebunov Y.V., Kirtaev R.V., Ermolaev G.A., Mironov M.S., Novikov S.M., Arsenin A.V., Volkov V.S. *Adv. Mater. Interfaces*, **6**, 1900196 (2019).